Gerben P. Krielaart, Marcel Onink, Kees M. Brakman, Frans D. Tichelaar, Eric J. Mittemeijer and Sybrand van der Zwaag

(Laboratory of Materials Science, Delft University of Technology, Rotterdamseweg 137, 2628 AL Delft, The Netherlands)

Thermodynamic Analysis of Isothermal Transformations of Hypo-eutectoid Fe–C Austenites

The thermodynamics of decomposition reactions of undercooled austenite in Fe–C alloys were studied using a regular solution sublattice model for austenite and ferrite and taking cementite as a stoichiometric compound. From a Gibbs free energy point of view intermediate transformations, not leading to stable phases, are possible: carbide formation above the A_1 temperature, and carbon enrichment in austenite below the A_1 temperature. The differences in chemical potential of Fe and of C between both sides of the transformation front were calculated as a function of the degree of transformation and related to the kinetics of transformation interface progress and carbon rearrangement, respectively. Experimental evidence for the occurrence of carbide formation above the A_1 temperature was obtained. A thermodynamic calculation of the onset of the pearlite formation in hypoeutectoid Fe–C alloys is presented.

1 Introduction

The transformation from austenite to ferrite is the principal phase transformation of technological interest in steel production, in particular of low alloy construction steels. Despite numerous studies the austenite/ferrite phase transformation in Fe–C alloys is still not completely understood. Since the solubility of C in ferrite is very low, the formation of ferrite not only requires a transformation of the Fe lattice from an fcc (γ) to a bcc (α) crystal structure, but also the diffusion of C away from the ferrite nucleus: the remaining austenite enriches in C. Although the quantitative relation between the thermodynamics and the kinetics of a phase transformation is unknown, it is tempting to consider the mobility of the transformation interface as the consequence of the difference in the chemical potential of Fe between ferrite (α) and austenite (γ) at the interface [1]. The rearrangement of C can be conceived as the consequence of the difference in the chemical potential of C between ferrite and austenite at the interface. Against this kinetic background it is interesting to consider the chemical potential differences between ferrite and austenite upon progressive transformation.

Attempts have been made, starting in the 60's [2], to link the thermodynamics of the Fe–C system with the kinetics of the transformations in different temperature regions. No quantitative agreement was achieved [3 to 7]. In such treatments, it has often been assumed that so-called local equilibrium [8] prevails at the moving α/γ interface [7, 9 to 11]. This concept requires that for both phases the chemical potentials of Fe and those of C at both sides of the moving interface should be equal. As a consequence the C concentration of the austenite at the interface should be equal to the concentration indicated by the $(\gamma+\alpha)/\gamma$ phase boundary in the Fe–C phase diagram, irrespective of the degree of transformation.

Recently, deviations from the local equilibrium concept have been applied to describe the formation of bainite [12, 13]. Massive transformation prior to diffusional transformation is suggested by [14] allowing non-equilibrium concentrations of carbon in austenite and ferrite at the interface at early stages of the transformation. Recently, employing microscopical, diffraction and dilatometric techniques, experimental evidence was obtained indicating that local equilibrium appears not to be valid for intermediate stages of the austenite/ferrite transformation, at least not in pure Fe–C alloys [15]. Hence, in this paper the local equilibrium concept is not imposed. A primitive model presented here for the non-equilibrium carbon concentration at the interface can already explain experimental results obtained in this work. The carbon concentration of the austenite at the interface is allowed to vary with the stage of the transformation.

2 Transformations

Thermodynamic calculations are presented for the case that the alloys are quenched from the austenite single-phase field to a suitable temperature where the transformation proceeds; it is taken that no transformation takes place during the quench. Two different transformation reactions are considered:

Transformation 1. Decomposition of the supersaturated austenite (γ_χ) into (pro-eutectoid) ferrite (α) and C enriched austenite ($\gamma_{\chi'}$)

$$\gamma_\chi \rightarrow \alpha + \gamma_{\chi'}$$

where χ and χ' denote the atom fractions of C in the austenite prior to and during (after) transformation, respectively. According to the mass balance, the mean carbon atom fraction in the austenite increases from χ to χ' by:

$$\chi' = \frac{\chi - f \cdot \chi_\alpha}{1-f} \qquad (1)$$

where χ_α is the atom fraction of carbon in ferrite and where f is the fraction of the atoms incorporated in the transformation product ferrite. The compositions of ferrite

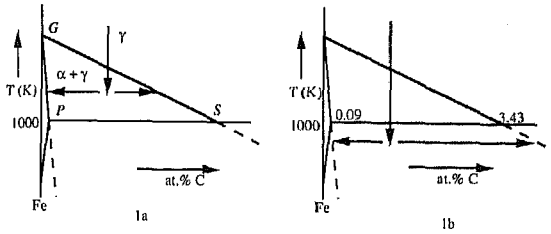

Fig. 1. Illustration in schematic Fe–C phase diagrams of austenite decomposition in ferrite and carbon enriched austenite, $\gamma_\chi \rightarrow \alpha + \gamma_{\chi'}$, above the A_1 temperature (reaction (1a)) and below the A_1 temperature (reaction (1b)). The A_1 temperature is taken as 1000 K.

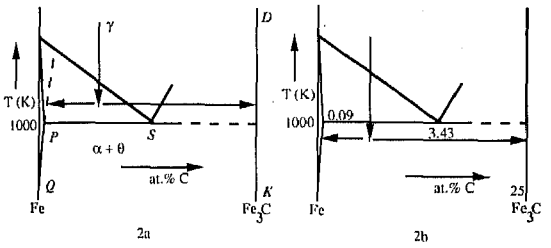

Fig. 2. Illustration in schematic Fe–C phase diagrams of austenite decomposition in ferrite and cementite, $\gamma_\chi \rightarrow \alpha + \theta$, above the A_1 temperature (reaction (2a)) and below the A_1 temperature (reaction (2b)). The A_1 temperature is taken as 1000 K.

and austenite after completed transformations are given by the (extrapolated) GP and (extrapolated) GS phase boundaries of the Fe–C phase diagram, respectively (Fig. 1) [16]. If the reaction takes place above the A_1 temperature (1000 K) it is denoted by (1a). If the reaction takes place below A_1 it is denoted by (1b).

Transformation 2. Decomposition of the supersaturated austenite into ferrite and cementite (θ):

$$\gamma_\chi \rightarrow \alpha + \theta$$

The compositions of ferrite and cementite are given by the (extrapolated) PQ and DK phase boundaries of the Fe–C diagram, respectively (Fig. 2). If the reaction takes place above A_1 it is denoted by (2a). If the reaction takes place below A_1 it is denoted by (2b).

3 Thermodynamic Model

3.1 Gibbs Free Energies and Chemical Potentials

3.1.1 Austenite and Ferrite; the Regular Solution Sublattice Model

In order to account for the dependence of the Gibbs free energy on the carbon concentration, the following description is adopted. Austenite and ferrite can be conceived as constituted of two interpenetrating sublattices: the M sublattice, fully occupied by Fe atoms, and the I sublattice, occupied by a mixture of C atoms and vacancies (V). The I sublattice is formed by the octahedral interstices of the M sublattice. The following contributions to the Gibbs free energy can be distinguished: the Gibbs free energy of the pure component M, the Gibbs free energy of the substitutional binary alloy C–V and the Gibbs free energy due to the interactions of M and C and of M and V. Including a pair-wide interaction of nearest neighbours on the sublattice occupied by C and V (leading to an excess enthalpy term described by the interaction parameter $L_{C,V}$) while maintaining a random distribution of C and V on the I sublattice (leading to the Gibbs expression for the entropy of ideal mixing), the total Gibbs free energy, G_m, according to the regular solution sublattice model [17 to 19], for one mole of $Fe(C_y V_{1-y})_{c/a}$ is given by:

$$G_m = (1-y)G^0_{Fe} + y \cdot G^0_{FeC_{c/a}} + y(1-y) \cdot \frac{c}{a} \cdot L_{C,V} + RT\frac{c}{a}\{y \ln y + (1-y) \ln (1-y)\} \quad (2)$$

where c/a denotes the ratio of the number of I sublattice sites and the number of M sublattice sites and y designates the site fraction of C on the I sublattice that can be calculated from the atom fraction of C in the Fe–C alloy, x, according to

$$y = \frac{a}{c}\frac{x}{1-x} \quad (3)$$

G^0_{Fe} represents the Gibbs free energy for one mole of pure Fe (with M-type lattice). Terms containing the Gibbs free energy of one mole of V, G^0_V, have been omitted since obviously, $G^0_V \equiv 0$. $G^0_{FeC_{c/a}}$ is the Gibbs free energy of one mole of $FeC_{c/a}$. Values for $G^0_{FeC_{c/a}}$ and $L_{C,V}$ result from fitting of calculated phase diagrams to experimental data and cannot be determined experimentally in a direct way [20]. In the case of ferrite, the Gibbs free energy of the pure Fe is affected by the change in magnetic state on passing the ferromagnetic transition temperature, T_C. The ferromagnetic contribution to the Gibbs free energy of ferrite is considered to be independent of the C concentration [20] and its temperature dependence is well approximated by a polynomial valid below T_C and a polynomial valid above T_C [20, 21]. Numerical data for the calculation of the Gibbs free energies of ferrite and austenite according to Eq. (2) are provided in Tables A1a, b, d and e (see Appendix).

The Gibbs free energy of one mole of the binary mixture $Fe(C_y V_{1-y})_{c/a}$ can formally be written as:

$$G_m = \mu_{Fe} + y \cdot \frac{c}{a} \cdot \mu_C \quad (4)$$

with μ_{Fe} and μ_C as the chemical potentials of Fe and C, respectively (recognising $\mu_V \equiv 0$). Then, by rewriting of Eq. (2) it follows that:

$$\mu_{Fe} = G^0_{Fe} + \frac{c}{a} \cdot y^2 \cdot L_{C,V} + \frac{c}{a} RT \ln (1-y) \quad (5)$$

and:

$$\mu_C = \left\{\frac{a}{c} G^0_{FeC_{c/a}} - \frac{a}{c} G^0_{Fe} + L_{C,V}\right\} - 2 \cdot y \cdot L_{C,V} + RT \ln \frac{y}{1-y} \quad (6)$$

3.1.2 Cementite

Cementite is taken as a stoichiometric compound: Fe_3C. Numerical data for the calculation of the Gibbs free energy for cementite are listed in Table A1c (see Appendix).

3.2 Total Gibbs Free Energy Change

The chemical Gibbs free energy change, ΔG_{chem}, calculated for the completed transformation of one mole of $Fe(C, V)_{c/a}$ is defined as:

$$\Delta G_{chem} \equiv G_{final} - G_{start} \quad (7)$$

Thus it follows for:

Reactions (1a) and (1b):

$$\Delta G_{chem} = m_\alpha \cdot G_\alpha + m_{\gamma_{\gamma'}} \cdot G_{\gamma_{\gamma'}} - m_{\gamma_\gamma} \cdot G_{\gamma_\gamma} \quad (8)$$

Reactions (2a) and (2b):

$$\Delta G_{chem} = m_\alpha \cdot G_\alpha + m_\theta \cdot G_\theta - m_{\gamma_\gamma} \cdot G_{\gamma_\gamma} \quad (9)$$

where m_i denotes the number of moles of Fe in phase i, recognising that the initial stage is given by one mole of austenite of composition $FeC_{x(c/a)}$: $m_{\gamma_\gamma} = 1$. G_α, G_{γ_γ} and $G_{\gamma_{\gamma'}}$ are calculated using Eq. (2) and G_θ follows from Table A1c.

3.3 Chemical Potential Differences

Considering reaction (1), the chemical potential differences experienced at the moving α/γ interface during transformation are defined as follows:

$$\Delta\mu_{Fe} \equiv (\mu^\alpha_{Fe})_{\alpha/\gamma} - (\mu^\gamma_{Fe})_{\gamma/\alpha} \quad (10)$$

and:

$$\Delta\mu_C \equiv (\mu^\alpha_C)_{\alpha/\gamma} - (\mu^\gamma_C)_{\gamma/\alpha} \quad (11)$$

where $(\mu^\alpha_i)_{\alpha/\gamma}$ is defined as the chemical potential of component i in ferrite at the α/γ interface, etc. Obviously, after completed transformation both $\Delta\mu_{Fe}$ and $\Delta\mu_C$ are nil, because equilibrium has been reached throughout the entire specimen.

The local equilibrium model implies that $\Delta\mu_{Fe}$ and $\Delta\mu_C$ are nil at the interface during the entire transformation (see Sect. 1). Obviously, this is physically unrealistic. Under local equilibrium conditions there would be no driving force for the (net) transport of carbon across the interface; see also discussion in [14]. In particular during initial stages of the transformation significant deviations from local equilibrium may occur. In order to calculate $\Delta\mu_C$ and $\Delta\mu_{Fe}$ during the transformation, an assumption on the carbon redistribution has to be made. In the absence of reliable data, crude estimates have to be made for the carbon concentration in both phases at the interface. This approach seems acceptable in view of the qualitative conclusions to be reached (see discussion of results in Sect. 4.2).

The solubility of carbon in ferrite is very small and it is assumed here that the carbon concentration in α at the α/γ interface equals the (very small) equilibrium value (i.e.: the value prescribed by the accepted Fe-C phase diagram: $[C]^\alpha_{eq}$). The chemical potential of carbon in ferrite then equals the equilibrium value for both ferrite and austenite (cf. Figs. 3a and b). During transformation, the occurring carbon enrichment of the austenite involves that a carbon chemical potential difference exists between the γ/α interface and the interior of the γ grain, which drives the diffusion of carbon from the interface into the γ grain. The migration rate of the γ/α interface, the diffusion rate of C in austenite and the austenite grain size determine the time dependence of the carbon concentration in γ at the γ/α interface. Usually, this is modelled assuming local equilibrium at the γ/α interface, $(\mu^\alpha_C)_{\alpha/\gamma} = (\mu^\alpha_C)_{eq} = (\mu^\gamma_C)_{\gamma/\alpha} = (\mu^\gamma_C)_{eq}$, in which case the driving force for carbon diffusion in austenite is related to line segment (a) in Fig. 3b. Non-equilibrium conditions can prevail in practice. Then, the carbon concentration at the interface in the austenite and the corresponding chemical potential can be lower than as prescribed by equilibrium. Thus the driving force for carbon transport across the interface is related to line segment (b), while the driving force for diffusion of carbon in the austenite is related to line segment (d). Modelling of the carbon concentration profiles, using either local equilibrium or non-equilibrium conditions, is beyond the scope of this paper. To account for the non-equilibrium situation at the α/γ interface, it is assumed here that the carbon concentration in γ at the γ/α interface equals the (degree of transformation, i.e. time, dependent) average carbon concentration of the austenite, $\langle[C]^\gamma\rangle$, (see discussion in Sect. 4.2). Gradients in the carbon concentration, which will certainly occur during the transformation process, are neglected. Thus, on the basis of Eq. (11), the driving force for the rearrangement of carbon, which equals line segment (b), is approximated by line segment (c) (Fig. 3b).

The carbon rearrangement (leading to a certain carbon concentration in γ at the γ/α interface) has an effect on $\Delta\mu_{Fe}$ (and thus on the interface velocity, cf. Sect. 1) through the presence of the carbon concentration in Eq. (5). In the following the changes of $\Delta\mu_{Fe}$ and $\Delta\mu_C$ are discussed as a function of the fraction, f, of the atoms incorporated in the transformation product ferrite.

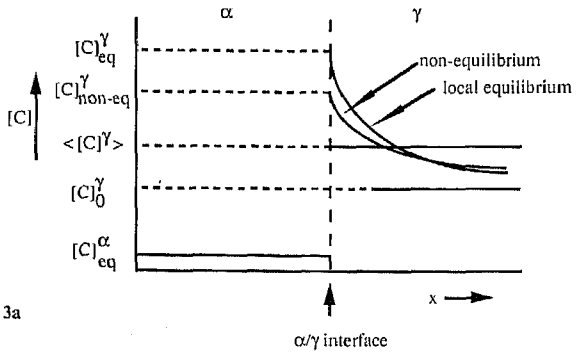

Fig. 3a. Schematic carbon concentration profiles at both sides of the ferrite (α) austenite (γ) interface for an intermediate stage of the transformation. At the interface the carbon concentrations for both the non-equilibrium situation, $[C]^\gamma_{non\text{-}eq}$, and the local equilibrium situation, $[C]^\alpha_{eq}$ and $[C]^\gamma_{eq}$, have been illustrated. The time dependent average carbon concentration in austenite is $\langle[C]^\gamma\rangle$; the initial carbon concentration is depicted as $[C]^\gamma_0$.

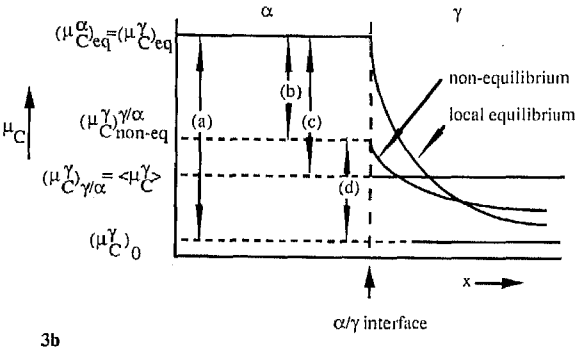

Fig. 3b. Schematic chemical potentials of carbon at both sides of the ferrite (α) austenite (γ) interface, corresponding to the carbon concentration profiles sketched in (a) $(\mu^\gamma_C)^{\gamma/\alpha}_{non\text{-}eq}$ is the non-equilibrium chemical potential of carbon in the austenite at the interface; $(\mu^\alpha_C)_{eq}$ and $(\mu^\gamma_C)_{eq}$ are the chemical potentials of carbon in austenite and in ferrite under the assumption of local equilibrium, $(\mu^\gamma_C)_0$ and $\langle\mu^\gamma_C\rangle$ represent the initial and average chemical potential of carbon in austenite, respectively.

4 Results and Discussion

4.1 Total Gibbs Free Energy Changes

The total chemical Gibbs free energy changes for the decomposition of austenite into ferrite and carbon enriched austenite are shown as a function of temperature in Fig. 4 for Fe–C alloys with a carbon concentration ranging from 0.0 to 0.8 mass%. Similarly, the total chemical Gibbs free energy changes for the decomposition of austenite into ferrite and cementite are shown in Fig. 5 as a function of temperature for Fe–C alloys with a carbon concentration ranging from 0.0 to 0.8 mass%. For these calculations the carbon concentrations in ferrite, below A_1 for transformation (1b) and above A_1 for transformation (2a), have been taken in accordance with the extrapolated phase boundaries GP and PQ, respectively (see Figs. 1 and 2 and Table A2). If these carbon concentrations are taken equal to those indicated by the corresponding equilibrium phase boundaries (PQ and GP, respectively), no significant changes occur in the calculated values for ΔG_{chem}.

Obviously, from a comparison of the ΔG_{chem} values it is seen that at temperatures above A_1 ferrite formation with associated carbon enrichment of the austenite (reaction (1a)) will lead to the most stable configuration, whereas at temperatures below A_1 formation of ferrite together with cementite (reaction (2b)) will lead to the most stable configuration. However, from the energy point of view, the metastable transformations (1b) (below A_1) and (2a) (above A_1) are also possible. The decomposition of undercooled austenite into ferrite and carbon enriched austenite leads in all cases to a decrease of the Gibbs free energy of the system at temperatures below A_1 (reaction (1b); see also [2]). The decomposition of undercooled austenite into ferrite and cementite above A_1 (reaction (2a)) only leads to a decrease of the Gibbs free energy of the system for limited ranges of temperature and carbon concentration (see Fig. 5).

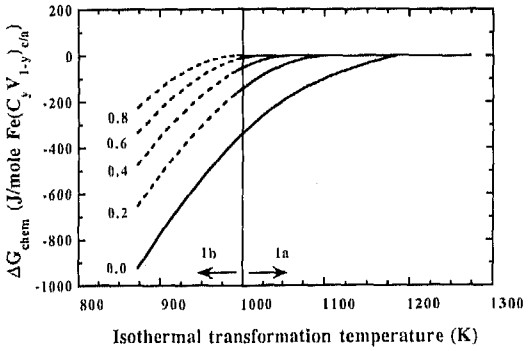

Fig. 4. The total Gibbs free energy change as a function of isothermal transformation temperature for the decomposition of austenite according to $\gamma_\chi \rightarrow \alpha + \gamma_{\chi'}$ for various carbon concentrations in mass% (Eq. (8)). Reaction (1a) above A_1: solid lines. Reaction (1b) below A_1: dashed lines.

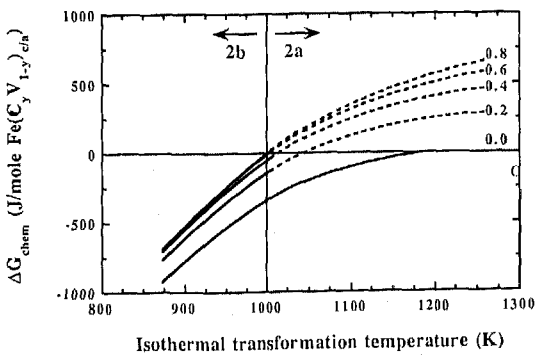

Fig. 5. The total Gibbs free energy change as a function of isothermal transformation temperature for the decomposition of austenite according to $\gamma_\chi \rightarrow \alpha + \theta$ for various carbon concentrations in mass% (Eq. (9)). Reaction (2a) above A_1: solid lines. Reaction (2b) below the A_1: dashed lines.

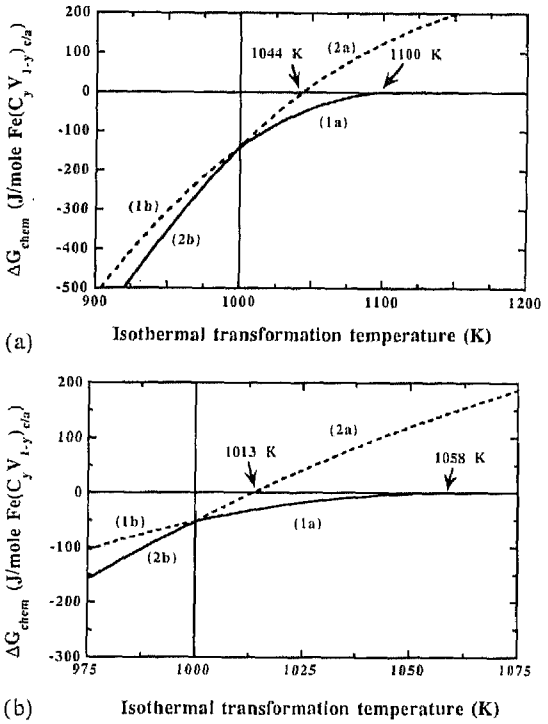

Fig. 6a and b. Comparison of total Gibbs free energy changes for reactions (1a and b) ($\gamma_\chi \rightarrow \alpha + \gamma_{\chi'}$) and (2a and b) ($\gamma_\chi \rightarrow \alpha + \theta$) as a function of isothermal transformation temperature for carbon concentrations 0.2 mass% (a) and 0.4 mass% (b).

The Gibbs free energy changes for all four reactions can be compared for alloys with carbon concentrations of 0.2 mass% C and 0.4 mass% C in Figs. 6a and 6b. Clearly, in particular below A_1, the thermodynamically less preferred transformation (reaction (1b)) already provides (far) more than half of the energy gain due to the thermodynamically preferred transformation (reaction (2b)). A similar statement can be made concerning the situation above A_1, although for the alloys given it only holds below a certain temperature (well below 1044 K and 1013 K for 0.2 mass% C and 0.4 mass% C, respectively). The locus of $\Delta G_{chem} = 0$, for reaction (2a) (see Figs. 6a and 6b) provides a metastable phase boundary in the Fe–C diagram for the transformation of undercooled austenite into ferrite and cementite above A_1; it is shown in Fig. 7.

Because a net Gibbs free energy gain can occur yet, kinetic reasons can induce the thermodynamically less favoured transformations (1b) and (2a). Below A_1 carbon enrichment of austenite is possible. Similarly, above A_1 the formation of metastable carbide is possible. When such carbide precipitation occurs, the α/γ interface may become pinned by the carbide particles. At this place it should be recalled that for the sake of simplicity it was assumed that the carbon in the remaining austenite is distributed homogeneously. This is

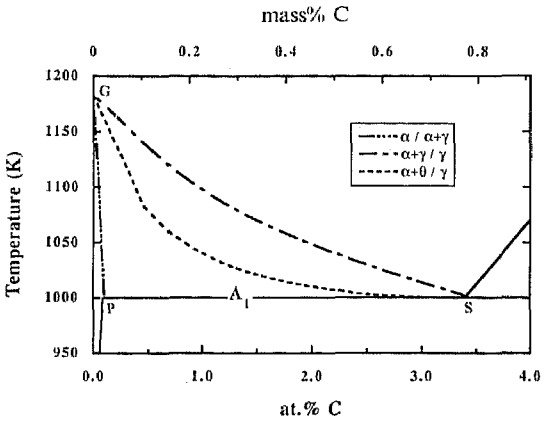

Fig. 7. Part of the Fe–C phase diagram showing the calculated metastable $(\alpha + \theta)/\theta$ phase boundary.

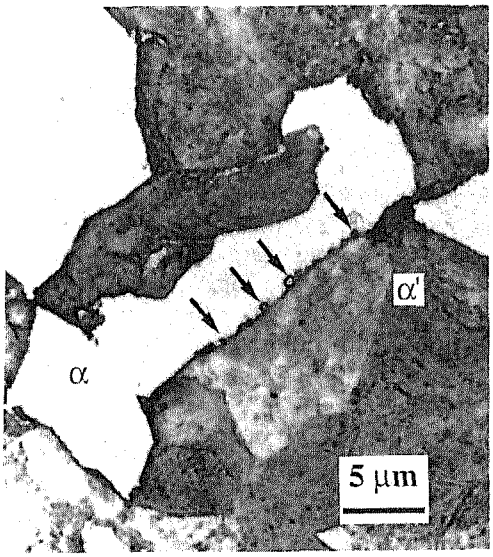

Fig. 8. Optical micrograph (bright field, oil immersion) of an Fe-0.36 mass% C alloy after (partial) transformation at 1005 K during 30 s. Because of the quench to room temperature the austenite phase was transformed into martensite. At the ferrite/martensite interface small precipitates (see arrows) can be discerned.

compatible with a migration rate that is slow with respect to the diffusion rate of carbon in austenite.

4.1.1 Experimental Observations

Experiments demonstrate that below A_1 pro-eutectoid ferrite formation (i.e. reaction (1b)) can occur before pearlite formation takes place [24] (see also the theoretical and experimental results presented in Sect. 4.2). To our knowledge, evidence for the occurrence of carbide formation in hypo-eutectoid Fe–C alloys above A_1 (reaction (2a)) has not been presented until now. Experimental data obtained in this work suggest that reaction (2a) is possible.

Thin-walled specimens (0.25 mm thickness) of high purity Fe–C alloys containing 0.17 mass% C (and (numbers denote mass%) 0.001 Cr; 0.007 Cu; 0.0007 Mn; 0.001 Mo; 0.004 Ni; 0.001 Sn) and 0.36 mass% C (0.001 Cr; 0.015 Cu; 0.0007 Mn; 0.001 Mo; 0.003 Ni; 0.001 Sn) were isothermally transformed above A_1 at 1005 K, i.e. within the hypothetical $\alpha + \theta$ region (see dashed line in Fig. 7). The specimens were quenched to room temperature after partial (about 70 %) or completed transformation. For experimental details see [15]. Optical analysis of the microstructure obtained showed the presence of the phases to be expected: ferrite (transformation product phase) and martensite (former austenite which transformed during quenching to room temperature).

However, in addition unusual precipitates were observed at the majority of the ferrite/martensite interfaces. A typical example is shown in Fig. 8. The size of the precipitates is about 200 nm, which is close to the resolution of the optical microscope. Etching with Murakami etchant, which stains carbides, supports the interpretation that the precipitates formed are carbides.

4.2 Chemical Potential Differences during Transformation

The chemical potential differences $\Delta\mu_{Fe}$ and $\Delta\mu_C$, as defined according to Eqs. (10) and (11), have been devised to envisage energy changes for iron and carbon individually at the α/γ interface. They can be calculated along the lines discussed in Sect. 3.3 as a function of the fraction of ferrite formed. A negative value for $\Delta\mu_{Fe}$ drives the transformation from $\gamma \rightarrow \alpha$ and a positive value for $\Delta\mu_C$ indicates carbon uptake by the austenite (see also Table 1). Note that as a consequence of the definition of f (= fraction of the atoms incorporated in the transformation product ferrite), the value of f for completed transformation will be smaller than one for all alloys.

The fraction f reached when $\Delta\mu_{Fe} = 0$ and $\Delta\mu_C = 0$ are plotted vs. temperature in Figs. 9a,b and 10a,b for 0.2 mass% C and 0.4 mass% C, respectively. Regions in these figures where $\Delta\mu_{Fe}$ and $\Delta\mu_C$ are positive or negative have been designated by + and − signs.

Table 1. Chemical potential differences and associated processes.

$\Delta\mu_{Fe}$			$\Delta\mu_C$	
>0	=0	<0	>0	=0
interface migration into ferrite	no transformation	interface migration into austenite: formation of ferrite (1a), (1b') or pearlite formation (2b)	C uptake by remaining austenite (1a), (1b')	no transformation (1b) or pearlite formation (2b)

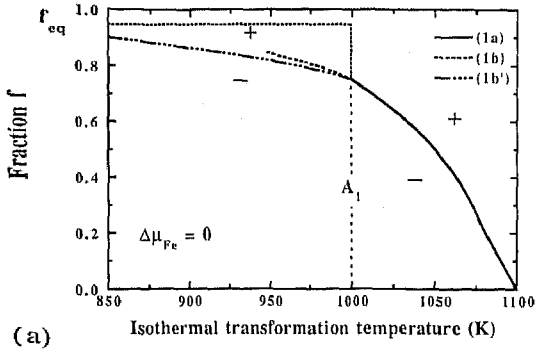

(a)

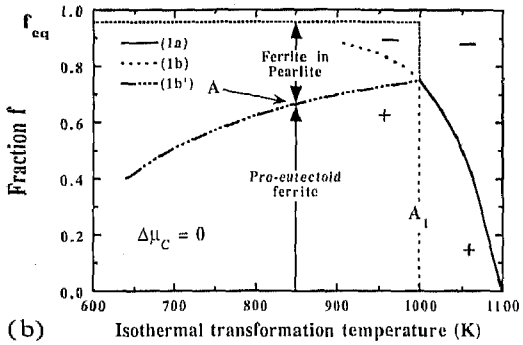

(b)

Fig. 9a and b. (a): The fraction f of the atoms incorporated in the transformation product ferrite for an Fe-0.2 mass% C alloy as a function of isothermal transformation temperature for $\Delta\mu_{Fe} = 0$ (cf. Eq. (9)) for austenite decomposition according to $\gamma_\chi \rightarrow \alpha + \gamma_{\chi'}$ above A_1 (reaction 1(a)) and below A_1 (reaction (1b)). The result for reaction (1b') (see text) has been presented too. The signs + and − indicate regions in the diagram where $\Delta\mu_{Fe} > 0$ and $\Delta\mu_{Fe} < 0$, respectively; (b): as (a) but for $\Delta\mu_C$, (Eq. (11)).

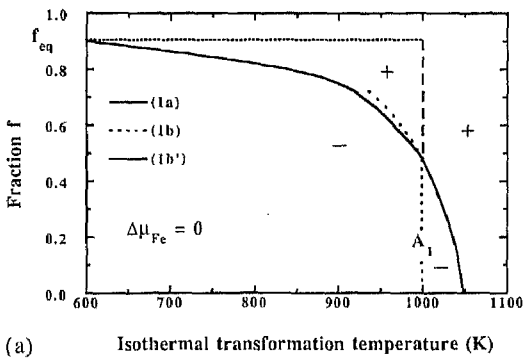

(a)

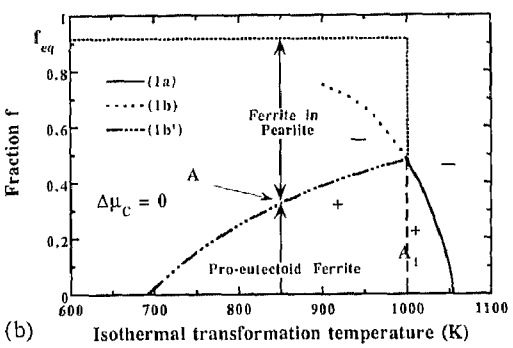

(b)

Fig. 10a and b. (a): The fraction f of the atoms incorporated in the transformation product ferrite for an Fe-0.4 mass% C alloy as a function of isothermal transformation temperature for $\Delta\mu_{Fe} = 0$ (cf. Eq. (10)) for austenite decomposition according to $\gamma_\chi \rightarrow \alpha + \gamma_{\chi'}$ above A_1 (reaction 1(a)) and below A_1 (reaction (1b)). The result for reaction (1b') (see text) has been presented too. The signs + and − indicate regions in the diagram where $\Delta\mu_{Fe} > 0$ and $\Delta\mu_{Fe} < 0$, respectively; (b): as (a) but for $\Delta\mu_C$, (Eq. (11)).

Clearly for reaction (1a) both $\Delta\mu_{Fe}$ and $\Delta\mu_C$ favour the formation of ferrite combined with carbon enrichment of the remaining austenite ($\Delta\mu_{Fe} < 0$; $\Delta\mu_C > 0$). For temperatures above A_1, on increasing f (from zero) $\Delta\mu_{Fe}$ gradually becomes less negative due to the increase of the carbon concentration χ' in the austenite. The fractions f for reaction (1a) at which the driving forces for interface migration ($\Delta\mu_{Fe}$) and carbon rearrangement ($\Delta\mu_C$) become nil, are exactly the same, and this occurs when the equilibrium fraction of ferrite, as indicated by the Fe–C phase diagram (see Fig. 11a), has been formed.

From the energy point of view, at temperatures below A_1 reaction (1b) may occur because of kinetic preference (cf. Sect. 4.1). Now, the fraction f reached when $\Delta\mu_{Fe} = 0$ for reaction (1b) is smaller than that indicated by the accepted equilibrium phase diagram for completed transformation (the latter value, f_{eq}, is indicated by the nearly horizontal lines in Figs. 9a,b and 10a,b). For these calculations the assumed carbon concentration in ferrite for reaction (1b) was obtained by extrapolation of the values for the equilibrium carbon solubility in ferrite above A_1 (Table A2). However, the maximum solubility of carbon in ferrite according to the accepted phase diagram below A_1 is lower than this value (cf. Fig. 2a and Fig. 1a: PQ vs. extrapolation of GP). Adopting the carbon solubility in ferrite as indicated by the accepted phase diagram below A_1, the calculations of $\Delta\mu_{Fe}$ and $\Delta\mu_C$ were also performed. The results are denoted as (1b') in the figures. Obviously, the effect on $\Delta\mu_{Fe}$, and thus on the values of f reached when $\Delta\mu_{Fe} = 0$, is of minor importance. However, the locus of points (in the f–T diagrams) where $\Delta\mu_C = 0$ is affected pronouncedly. Now consider Figs. 9b and 10b. The vertical lines drawn at 850 K indicate an isothermal transformation of undercooled austenite starting from the abscissa (where the fraction of ferrite is zero; fully austenitic state). Initially, the chemical potential difference for carbon is strongly positive, favouring carbon uptake by the austenite. According to reaction (1b') carbon uptake could thus occur until the point A is reached at which $\Delta\mu_C = 0$. At this stage, $\Delta\mu_{Fe}$ is still strongly negative (see Figs. 9a and 10a), providing a driving force for α/γ interface migration, i.e. favouring the continued formation of ferrite. However, beyond point A further carbon uptake by the austenite cannot take place. In other words: the Gibbs free energy change for the system for transformation (1b') is still negative, because it is governed by $\Delta\mu_{Fe}$, but $\Delta\mu_C$ opposes further carbon enrichment of the austenite. This result is interpreted here as that the condition $\Delta\mu_C = 0$ terminates reaction (1b'). Beyond point A the transformation continues as a reaction (2)-like eutectoid transformation: formation of pearlite. The ferrite formed at temperatures below A_1 before $\Delta\mu_C = 0$ according to reaction (1b') is denoted as pro-eutectoid ferrite. Hence, the transformation process at temperatures below A_1 can consist of two successive processes. First the transformation of γ_χ to $\alpha + \gamma_{\chi'}$ (1b') takes place, which is followed by transformation of $\gamma_{\chi'}$ to $\alpha + \theta$ (2b) from the moment, according to this work, that $\Delta\mu_C = 0$ (see also Table 1). The driving force for the eutectoid transformation is provided

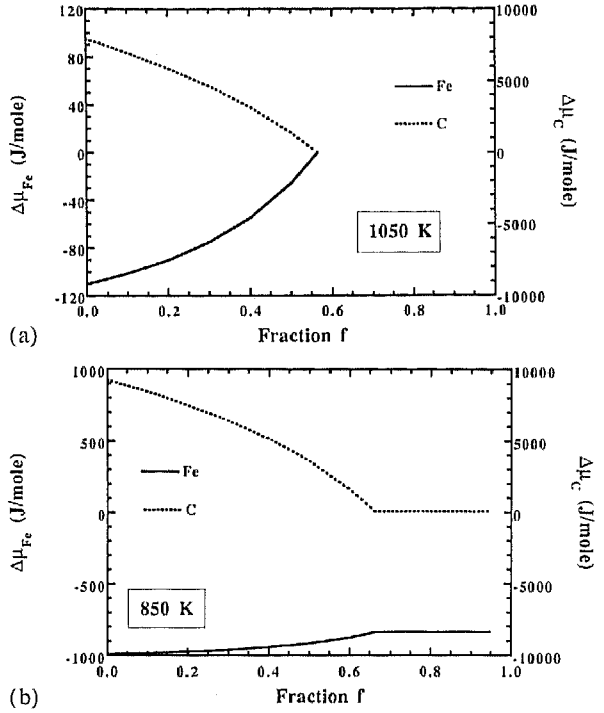

Fig. 11a and b. The chemical potential differences $\Delta\mu_{Fe}$ and $\Delta\mu_C$ (see Eqs. (10) and (11)) as a function of the fraction f of the atoms incorporated in the transformation product ferrite for the decomposition of austenite for a Fe-0.2 mass% C alloy during isothermal transformation at 1050 K, where reaction (1a) proceeds ($\gamma_\chi \rightarrow \alpha + \gamma_{\chi'}$) (a); at 850 K, where two reactions occur successively: $\gamma_\chi \rightarrow \alpha + \gamma_{\chi'}$ (reaction (1b')) and, at the moment that $\Delta\mu_C$ has become nil, $\gamma_{\chi'} \rightarrow \alpha + \theta$ (reaction (2b)) (b).

by $\Delta\mu_{Fe}$ only; $\Delta\mu_C$ remains zero and because no further carbon uptake of the remaining austenite occurs, $\Delta\mu_{Fe}$ remains constant until all austenite is transformed (see Fig. 11b; during this process, ferrite and cementite are assumed to be in equilibrium).

The total amount of ferrite formed after completed transformation is a function of the gross carbon concentration of the alloy only, ignoring the very small dependence on temperature of the very small solubility of C in ferrite. An immediate consequence of the two step process below A_1 is that the ratio of pro-eutectoid ferrite and pearlite is not fixed, but depends on both the carbon concentration of the alloy and the isothermal transformation temperature, as the stage of the transformation for reaction (1b') where $\Delta\mu_C = 0$ depends on the temperature (see Figs. 9b and 10b): the fraction of pro-eutectoid ferrite at which $\Delta\mu_C = 0$ decreases with temperature and carbon concentration. For a sufficiently low isothermal transformation temperature and a sufficiently high carbon concentration, $\Delta\mu_C$ would already be negative before any ferrite is formed (see Fig. 10b for $T < 690$ K). This means that the eutectoid-like transformation (2b) occurs without a preceding transformation (1b'); the specimen transforms to a 100 % pearlitic, or at sufficient undercooling, bainitic, microstructure. The carbon concentration in the metastable austenite at the moment of the start of the pearlite formation at temperatures below A_1 can be calculated from the fraction of ferrite where $\Delta\mu_C$ equals zero. The $\Delta\mu_C = 0$ line thus obtained is shown in Fig. 12. The figure suggests that the result can be conceived as an extrapolation of the ES boundary in the Fe–C equilibrium diagram (the notion of an extrapolated ES phase boundary has been adopted before [22, 23]). However, the $\Delta\mu_C = 0$ line calculated is not really an extrapolation of the ES boundary in the sense that it would describe the $\gamma/(\gamma + \theta)$ equilibrium. The precise course of the $\Delta\mu_C = 0$ line depends on the assumptions made for the carbon concentration in α and γ at the transformation interface. The only point made here is that $\Delta\mu_C = 0$ can be the criterion for the transition, below the A_1 temperature, from reaction (1b) to reaction (2b).

The calculations presented above hold for pure Fe–C alloys. It may be argued that for steels, also containing other elements, the results presented here would not be valid (for example, segregation of the alloying elements, other than carbon, at the α/γ interfaces could affect appreciably the thermodynamics prevailing there (cf. Eqs. (10) and (11)).

4.2.1 Experimental Observations

TTT diagrams indicate that, depending on the undercooling, the formation of pro-eutectoid ferrite is followed by the formation of pearlite [24]. In the literature, kinetic factors have been suggested as the origin for this phenomenon. Nucleation of pearlite would be facilitated by pro-eutectoid ferrite [25] and in semi-empirical models [26] an incubation time for the pearlite reaction longer than that for the pro-eutectoid ferrite reaction was incorporated. In this work, the transition from pro-eutectoid ferrite formation to pearlite formation during isothermal transformation is ascribed to thermodynamics ($\Delta\mu_C = 0$) rather than to transformation kinetics.

Occurrence of the two step reaction below A_1 was investigated by analysing the carbon redistribution quantitatively in high purity (see Sect. 4.1) binary Fe-0.17 wt.% C specimens after partial transformation. A thin-walled specimen (0.25 mm thickness) of the alloy was austenitised at 1373 K for 10 min, quenched to 973 K and isothermally transformed for 5 s at this temperature, leading to a fraction transformed of about 35 %. The specimen was subsequently quenched to room temperature (cooling rate >400 K s^{-1} during the first second). The resultant microstructure (see Fig. 13a) is composed of ferrite (transformation product) and martensite (core of the former austenite grains; formed during the quench) and troostite (located in the former austenite between the martensite and the ferrite; troostite forms during the quench if the cooling rate is slightly lower

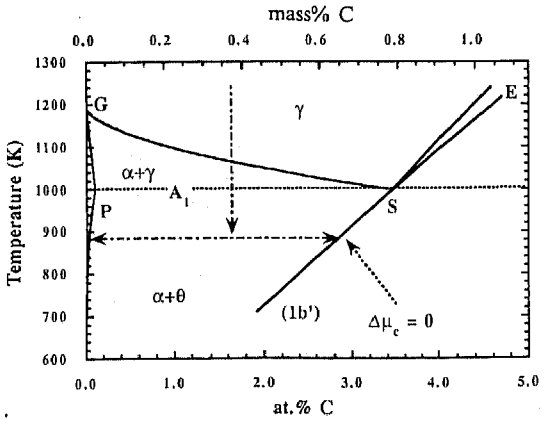

Fig. 12. Part of the Fe–C phase diagram showing the $\Delta\mu_C = 0$ line for reaction (1b').

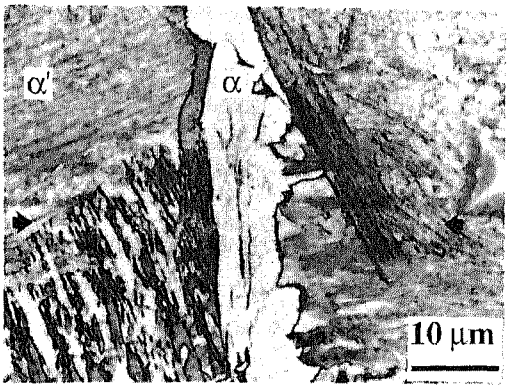

Fig. 13a. Optical micrograph (bright field, oil immersion) of an Fe-0.17 mass% C alloy after austenitising at 1373 K for 10 min, quench to and (partial) transformation at 973 K during approximately 5 s. The specimen is subsequently quenched to room temperature. Because of the quench to room temperature the austenite phase has become martensitic. Indications of a troostite- and Widmanstätten (ferrite) microstructure in the (former, i.e. before quenching) austenite phase at the ferrite/(former) austenite interface are observed. The arrows in the figure indicate the line-scan which is represented in (b).

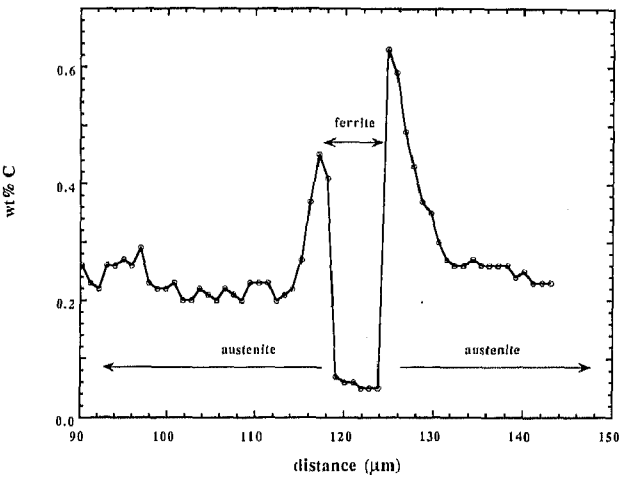

Fig. 13b. Carbon concentration profile across a remaining austenite grain for an Fe-0.17 mass% C alloy after partial (ca. 35%) transformation at 973 K for approximately 5 s. The carbon concentration data have been obtained by Electron-Probe Micro Analysis (EPMA) using wavelength dispersive spectrometers and a 10 kV electron beam of 100 nA, leading to a lateral resolution of less than 1 μm (for more details see [28]).

than a critical value above which only martensite forms [27][1]).

The corresponding carbon concentration profiles were measured applying electron-probe micro analysis (EPMA) with a counting statistical accuracy of 0.02 mass% C. The incident electron 10 keV beam had a lateral size of about 0.5 μm, which, according to Monte Carlo simulation for the paths of the electron beams, corresponds to an excited specimen volume of lateral size <0.8 μm, even not considering the effect of absorption of the emitted C Kα radiation which further reduces the lateral size (depth of information <0.3 μm) (for further details of measurement and evaluation see [28]). As follows from the carbon concentration profile shown in Fig. 13b, the carbon concentration in the γ at the γ/α interface (0.45 mass% C to 0.65 mass% C) is significantly larger than the initial carbon concentration in the austenite. The carbon concentration in the ferrite is larger than the equilibrium value (≈ 0.05 mass% C versus ≈ 0.02 mass% C); check measurements on pure Fe before and after the measurements on the specimens concerned suggest that the carbon concentration measured for the ferrite is reliable.

If local equilibrium would prevail, the carbon concentration in the austenite at the austenite/ferrite interface should have a value of about 1.0 mass% C (as follows from an extrapolation of the GS phase boundary in the Fe–C phase diagram according to the formula given in Table A2), which is significantly larger than the experimental value (0.45 to 0.65 mass% C). Considering the lateral resolution of the EPMA measurements (see above) and the carbon concentration profile in austenite near the interface, it may be argued that the carbon concentration in austenite at the interface is somewhat higher than the value read from the figure. However, it is very unlikely that this could explain the large difference with the prediction according to local equilibrium. According to all other (about 10) measurements performed, the carbon concentration in austenite at the austenite/ferrite interface never exceeded 0.65 mass% C before pearlite formation was observed. (Note that for the experiment concerned, the maximal carbon concentration in austenite before pearlite formation starts equals about 0.72 mass% C, according to the $\Delta\mu_C = 0$ criterion; see Fig. 12.) This leads to the conclusion that local equilibrium is not operative under the prevailing conditions.

Adopting the experimentally observed values for the carbon concentration in austenite at the austenite/ferrite interface, the driving force for interface migration, $\Delta\mu_{Fe}$, can be calculated (cf. Sect. 3.3) for the experiment discussed. It follows that $\Delta\mu_{Fe} = -200$ J/mol. The corresponding value of $\Delta\mu_C$, i.e. the driving force for carbon redistribution, is approximately 2300 J/mol. Recognising that there are many more Fe atoms than C atoms, it is concluded that an appreciable amount of the Gibbs free energy released by the phase transformation is used to drive the austenite/ferrite interface. This result, in conjunction with the observation of a carbon concentration profile within the austenite, leads to the conclusion that the kinetics of the austenite decomposition are controlled by both interface mobility and carbon diffusion within the austenite. The occurrence of local equilibrium would imply that the interface reaction is not of importance for the kinetics of the transformation [29].

The calculations in this paper were based on the assumption that the distribution of carbon in austenite is homogeneous. This crude approximation does not affect the general conclusions reached. However, it should be realised that the stage of transformation where $\Delta\mu_C = 0$ is determined by the specific change of the carbon concentration in the austenite at the interface upon progressive transformation (cf. Eq.

[1]) The occurrence of troostite at the austenite grain boundaries is a consequence of the relatively low cooling rate achieved by quenching with helium gas, in particular during the beginning of the quench [15]. The interpretation of the observed morphology as troostite formed during the quench (and not as some sort of very fine pearlite resulting from transformation at the transformation temperature beyond the stage indicated with A in Figs. 9b and 10b) is supported by the occurrence of this same troostite morphology at the austenite grain boundaries after quenching from transformation temperatures above A_1 (where pearlite cannot form at the transformation temperature), and the observation of Widmannstätten ferrite also present (which can only have been formed upon quenching).

(11)). Therefore this stage of transformation depends on the interface mobility, the austenite grain size and the temperature. The present estimate of the carbon concentration in austenite at the interface, equal to the average carbon concentration in the austenite, can be considered as an underestimate corresponding with an overestimate for the stage of transformation where pearlite formation starts.

5 Conclusions

Knowledge of the thermodynamic properties of ferrite, austenite and cementite, leads to the following conclusions about the α/γ transformation in Fe–C alloys:

(i) Because of the associated appreciable reduction in total Gibbs free energy, two intermediate transformations, not leading to the stable phase(s), can occur if they are favoured kinetically:
- below the A_1 temperature: decomposition of austenite in ferrite and carbon enriched austenite, followed by pearlite formation; as is well known from TTT diagrams.
- above the A_1 temperature: decomposition of austenite into ferrite and iron carbide for restricted ranges in temperature and carbon content.

Experimental results exist which are compatible with the occurrence of these intermediate transformations. From the total Gibbs free energy change, a metastable $(\alpha+\theta)/\gamma$ phase boundary above the A_1 temperature can be calculated.

(ii)
- Adopting the non-occurrence of local equilibrium, it is proposed that the decomposition of austenite into ferrite and carbon enriched austenite below the A_1 temperature occurs until $\Delta\mu_C = 0$. At that stage $\Delta\mu_{Fe}$ is still negative. Beyond this stage, austenite decomposition proceeds as an eutectoid transformation: pearlite forms. As a consequence the amount of pro-eutectoid ferrite is predicted to depend not only on gross carbon concentration but also on the transformation temperature. The eutectoid transformation continues until the whole specimen is transformed while $\Delta\mu_{Fe}$ remains constant and $\Delta\mu_C = 0$.
- The kinetics of the formation of pro-eutectoid ferrite upon austenite decomposition are controlled by both interface mobility and carbon diffusion within the austenite.

Appendix: Compilation of Thermodynamic Data

Contributions to the Gibbs free enrgy G_m for one mole $Fe(C, V)_{c/a}$ (see Eq. (1)) for ferrite and austenite are given in Tables A1a and A1b. The Gibbs free energy for cementite G_0 is given in Table A1c. $G^0_{graphic}$ is given in Table A1d. The data hold for temperature range: $298.15\ K < T < 1811\ K$. The reference states $H^{ref} = H_{298} - H_0$ and $S_{ref} = S_{298}$ for Fe and C are given in Table A1e.

Phase boundaries in the Fe–C diagram are presented in Table A2 by giving the corresponding carbon content as a function of temperature. Results labelled "this work" were obtained here by fitting to the data of [16].

The authors are indebted to Ir. W. G. Sloof for the Electron-Probe Micro Analysis (EPMA) and to Mr. P. F. Colijn for assistance with light microscopy. The authors are grateful to Prof. B. M. Korevaar for discussion. Financial support by Hoogovens Corporate Research, IJmuiden, The Netherlands, and the Innovative Research Project for Metals of the Dutch government (IOP-Metalen) is gratefully acknowledged.

Table A1a. Ferrite [20, 21]. G_{mag} indicates the ferromagnetic contribution; $\tau = T/T_C$ with T_C as the Curie temperature of ferrite. ($T_C = 1043$ K).

G^0_{Fe}	$1224.83 + 124.134 \cdot T - 23.5143 \cdot T \cdot \ln(T) - 0.00439752 \cdot T^2 - 5.89269 \times 10^{-8} \cdot T^3 + 77358.5 \cdot T^{-1} + \frac{1}{1-y} G_{mag} + H^{ref}_{Fe}$ (J/mol)
$G^0_{FeC_{c/a}}$	$322050 + 75.667 \cdot T + G^0_{Fe} + \frac{c}{a} \cdot G^0_{graphite}$ (J/mol)
G_{mag} ($\tau < 1$)	$-9180.5 + 9.723 \cdot T - 9309.8 \cdot \left(\frac{\tau^4}{6} + \frac{\tau^{10}}{135} + \frac{\tau^{16}}{600}\right)$ (J/mol)
G_{mag} ($\tau > 1$)	$-6507.7 \cdot \left(\frac{\tau^{-4}}{10} + \frac{\tau^{-14}}{315} + \frac{\tau^{-24}}{1500}\right)$ (J/mol)
$\frac{c}{a} L_{C,V}$	$-190 \cdot T$ (J/mol)
$\frac{c}{a}$	3

Table A1b. Austenite [20].

G^0_{Fe}	$-237.57 + 132.416 \cdot T - 24.6643 \cdot T \cdot \ln(T) - 0.00375752 \cdot T^2 - 5.89269 \times 10^{-8} \cdot T^3 + 77358.5 \cdot T^{-1} + H^{ref}_{Fe}$ (J/mol)
$G^0_{FeC_{c/a}}$	$77207 - 15.877 \cdot T + G^0_{Fe} + \frac{c}{a} G^0_{graphite}$ (J/mol)
$\frac{c}{a} L_{C,V}$	-34671 (J/mol)
$\frac{c}{a}$	1

Table A1c. Cementite [20].

G^0_0	$-10745 + 706.04 \cdot T - 120.6 \cdot T \cdot \ln(T) + H^{ref}_C + 3H^{ref}_{Fe}$ (J/mol)

Table A1d. Graphite [30].

$G^0_{graphite}$	$-17369 + 170.73 \cdot T - 24.3 \cdot T \cdot \ln(T) - 4.723 \times 10^{-4} \cdot T^2 + 2562600 \cdot T^{-1} - 2.643 \times 10^8 \cdot T^{-2} + 1.2 \times 10^{10} \cdot T^3 + H^{ref}_C$ (J/mol)

Table A1e. Reference states of Fe and C [20]. The subscripts refer to the corresponding temperature in K.

Element	Phase	$H_{298} - H_0$ (J/mol)	S_{298} (J/mol/K)
Fe	bcc at 298.15 K	4489	27.28
C	graphite at 298.15 K	1054	5.74

Table A2. Phase boundaries in Fe-C phase diagram. Carbon content in at.% as a function of temperature T in K.

Phase boundary	Temperature range	at.%	Source
$\gamma/(\alpha+\gamma)$	[873, 1273]	$5.47472 \times 10^2 - 1.38709 \cdot T + 1.18089 \times 10^{-3} \cdot T^2 - 3.37774 \times 10^{-7} \cdot T^3$	this work
$\alpha/(\alpha+\gamma)$	[873, 1273]	$6.5594 \times 10^{-1} - 5.5361 \times 10^{-4} \cdot T$	this work
$\alpha/(\alpha+\theta)$	[473, 1000]	$100 \times 10^{(1.05 - 4040/T)}$	[31]

Literature

1. *Turnbull, D.:* Trans AIME *191* (1951) 661–665.
2. *Kaufman, L.; Radcliffe, S. V.; Cohen, M.:* in: V. F. Zackay, H. I. Aaronson (eds.), Decomposition of Austenite by Diffusional Processes, John Wiley and Sons, New York (1962) 313.
3. *Rees, G. I.; Bhadeshia, H. K. D. H.:* Mater. Sci. Technol. *8* (1992) 985–993.
4. *Rees, G. I.; Bhadeshia, H. K. D. H.:* Mater. Sci. Technol. *8* (1992) 994–996.
5. *Reed, R. C.; Bhadeshia, H. K. D. H.:* Mater. Sci. Technol. *8* (1992) 421–435.
6. *Bhadeshia, H. K. D. H.:* Mater. Sci. Technol. *1* (1985) 497–504.
7. *Enomoto, M.:* ISIJ Intern. *32* (1992) 297–305.
8. *Zener, C.:* J. Appl. Phys. *20* (1949) 950–953.
9. *Ågren, J.:* Acta metall. *30* (1982) 841–851.
10. *Aaronson, H. I.; Enomoto, M.; Reynolds Jr., W. T.:* in: J. D. Embury; G. R. Purdy (eds.), Advances in Phase Transitions, Pergamon Press, Oxford (1988) 20.
11. *Crusius, S.; Höglund, L.; Knoop, U.; Inden, G.; Ågren, J.:* Z. Metallkd. *83* (1992) 729–738.
12. *Mujahid, S. A.; Bhadeshia, H. K. D. H.:* Acta metall. mater. *40* (1992) 389–396.
13. *Hillert, M.; Höglund, L.; Ågren, J.:* Acta metall. mater. *41* (1993) 1951–1957.
14. *Sahvén, A.:* Metall. Trans. A *24A* (1993) 1507–1516.
15. *Onink, M.; Brakman, C. M.; Tichelaar, F. D.; Mittemeijer, E. J.; vd Zwaag, S.:* Mater. Sci. Forum *163–165* (1994) 63–68.
16. *Kubaschewski, O.:* Iron Binary Phase Diagrams, Springer-Verlag, Berlin (1982) 23.
17. *Hillert, M.; Staffansson, L.-I.:* Acta Chem. Scand. *24* (1970) 3618–3626.
18. *Harvig, H.:* Acta Chem. Scand. *25* (1971) 3199.
19. *Sundman, B.; Ågren, J.:* J. Phys. Chem. Solids *42* (1981) 297–301.
20. *Gustafson, P.:* Scand. J. Metall. *14* (1985) 259–267.
21. *Hillert, M.; Jarl, M.:* Calphad *2* (1978) 227–238.
22. *Hultgren, A.:* Metallography on Tungsten Steels, John Wiley and Sons, New York (1920) 30.
23. *Hawbolt, E. B.; Chau, B.; Brimacombe, J. K.:* Metall. Trans. A *16A* (1985) 565–578.
24. *van der Voort, G. F.:* Atlas of Time-Temperature Diagrams for Irons and Steels, American Technical Publications, Hitchin (1992).
25. *Hillert, M.:* in: V. P. Zackay, H. I. Aaronson, (eds.), Decomposition of Austenite by Diffusional Processes, John Wiley and Sons, New York (1962) 197.
26. *Kirkaldy, J. S.:* Scand. J. Met. *20* (1991) 50–61.
27. *Habraken, L.; de Brouwer, J.-J.:* De Ferri Metallographia I, Presse Academiques Européennes, Brussel (1966) 338.
28. *Somers, M. A. J.; Colijn, P. F.; Sloof, W. G.; Mittemeijer, E. J.:* Z. Metallkd. *81* (1990) 33–43.
29. *Hillert, M.:* Metall. Trans. A *6A* (1975) 5–19.
30. *Gustafson, P.:* Trita-Mac-0236, Div. Phys. Met., Royal Inst. Techn. Stockholm, Sweden.
31. *Jehn, H.:* Gases and Carbon in Metals, Physik Daten 5–14, Karlsruhe (1981).

(Received January 10, 1994)